Inorg. Chem. **2008**, *47*, 6353−6363

Structural and Spectroscopic Impact of Tuning the Stereochemical Activity of the Lone Pair in Lead(II) Cyanoaurate Coordination Polymers via Ancillary Ligands

Michael J. Katz,[†] Vladimir K. Michaelis,[‡] Pedro M. Aguiar,[‡] Renante Yson,[§] Haiyan Lu,[§] Harini Kaluarachchi,[†] Raymond J. Batchelor,[†] Georg Schreckenbach,[‡] Scott Kroeker,*[,‡] Howard H. Patterson,*[,§] and Daniel B. Leznoff*[,†]

Department of Chemistry, Simon Fraser University, 8888 University Drive, Burnaby, BC, Canada V5A 1S6, Department of Chemistry, University of Manitoba, Winnipeg, MB, Canada R3T 2N2, and Department of Chemistry, University of Maine, Orono, Maine 04469

Received March 7, 2008

The reaction of $Pb(ClO_4)_2 \cdot xH_2O$, an ancillary ligand L, and two equivalents of $Au(CN)_2^-$ gave a series of crystalline coordination polymers, which were structurally characterized. The ligands were chosen to represent a range of increasing basicity, to influence the stereochemical activity (i.e., p-orbital character) of the Pb(II) lone pair. The Pb(II) center in [Pb(1,10-phenanthroline)$_2$][Au(CN)$_2$]$_2$ (**1**) is 8-coordinate, with a stereochemically inactive lone pair; all 8 Pb−N bonds are similar. The $Au(CN)_2^-$ units propagate a 2-D brick-wall structure. In [Pb(2,2′-bipyridine)$_2$][Au(CN)$_2$]$_2$ (**2**), the 8-coordinate Pb(II) center has asymmetric Pb−N bond lengths, indicating moderate lone pair stereochemical activity; the supramolecular structure forms a 1-D chain/ribbon motif. For [Pb(ethylenediamine)][Au(CN)$_2$]$_2$ (**3**), the Pb(II) is only 5-coordinate and extremely asymmetric, with Pb−N bond lengths from 2.123(7) to 3.035(9) Å; a rare Pb−Au contact of 3.5494(5) Å is also observed. The $Au(CN)_2^-$ units connect the Pb(ethylenediamine) centers to form 1-D zigzag chains which stack via Au−Au interactions of 3.3221(5) Å to yield a 2-D sheet. ^{207}Pb MAS NMR of the polymers indicates an increase in both the chemical shielding span and isotropic chemical shift with increasing Pb(II) coordination sphere anisotropy (from $\delta_{iso} = -2970$ and $\Omega = 740$ for **1** to $\delta_{iso} = -448$ and $\Omega = 3980$ for **3**). The shielding anisotropy is positively correlated with Pb(II) p-character, and reflects a direct connection between the NMR parameters and lone-pair activity. Solid-state variable-temperature luminescence measurements indicate that the emission bands at 520 and 494 nm, for **1** and **2**, respectively, can be attributed to Pb → L transitions, by comparison with simple [Pb(L)$_2$](ClO$_4$)$_2$ salts. In contrast, two emission bands for **3** at 408 and 440 nm are assignable to Au−Au and Pb−Au-based transitions, respectively, as supported by single-point density-functional theory calculations on models of **3**.

Introduction

The synthesis of coordination polymers has been of great interest in recent years because of their interesting topological structures and their associated physical properties.[1–3] In the modular synthesis of these polymers, building blocks that can incorporate a wide range of metals and bridging ligands can be chosen, thereby facilitating the design of specific structures with predefined properties.[4–10] In making such

* To whom correspondence should be addressed. E-mail: scott_kroeker@umanitoba.ca (S.K.), howardp@maine.edu (H.H.P.), dleznoff@sfu.ca (D.B.L.). Phone: 1-204-474-9335(S.K.), 1-207-581-1178(H.H.P.), 1-778-782-4887(D.B.L.). Fax: 1-204-474-7608 (S.K.), 1-207-581-1191 (H.H.P.), 1-778-782-3765 (D.B.L.).
† Simon Fraser University.
‡ University of Manitoba.
§ University of Maine.

(1) Batten, S., R.; Robson, R. *Angew. Chem., Int. Ed.* **1998**, *37*, 1460.
(2) Janiak, C. *Dalton Trans.* **2003**, 2781.
(3) Moulton, B.; Zaworotko, M. J. *Chem. Rev.* **2001**, *101*, 1629.
(4) Culp, J. T.; Matranga, C.; Smith, M.; Bittner, E. W.; Bockrath, B. *J. Phys. Chem. B* **2006**, *110*, 8325.
(5) Fang, Q.-R.; Zhu, G.-S.; Xue, M.; Sun, J.-Y.; Qiu, S.-L. *Dalton Trans.* **2006**, 2399.
(6) Han, H.; Zhang, S.; Hou, H.; Fan, Y.; Zhu, Y. *Eur. J. Inorg. Chem.* **2006**, 1594.
(7) Herrera, J.-M.; Pope, S. J. A.; Adams, H.; Faulkner, S.; Ward, M. D. *Inorg. Chem.* **2006**, *45*, 3895.
(8) Krawiec, P.; Kramer, M.; Sabo, M.; Kunschke, R.; Fröde, H.; Kaskel, S. *Adv. Eng. Mater.* **2006**, *8*, 293.

10.1021/ic800425f CCC: $40.75
Published on Web 05/29/2008

choices, factors taken into consideration include the coordination preference of the metals used and the geometry and denticity of both the bridging and the ancillary ligand (if any) on the metal.[1,3] In general, most ancillary ligands are innocent, playing the key role of controlling the dimensionality and topology of the final polymer by limiting the number of open coordination sites and their orientation.[11–20]

With $d^{10}s^2$ metal ions such as lead(II), which is a common component in a range of materials with nonlinear optical (NLO), ferroelectric, and semiconductor properties,[21–28] an additional element of structural control can be tuned: the stereochemical activity of the lone pair. If stereochemically active, the lone pair occupies and blocks a portion of the lead(II) coordination sphere, thereby effectively altering the orientation of the remaining coordination sites for bridging ligands to occupy; if inactive, a more symmetric geometry becomes available. An in-depth study of lead(II) coordination compounds attributed the presence or absence of a stereochemically active lone pair to several factors, including the Lewis-base character of the ancillary ligand and the degree of ligand to metal charge transfer.[29] From a theoretical perspective, more basic constituents around the lead(II) center induce more mixing of the 6p orbital with the 6s orbital, leading to a stereochemical lone pair. Using this as a basis, lead(II) structures can be categorized as hemi- or holodirectional. From X-ray crystallographic data, hemidirectional structures have physical evidence that the lone pair is stereochemically active, usually in the form of unusually asymmetric bond lengths around the coordination sphere of the lead(II) (Figure 1). Holodirectional lead(II) complexes show much more symmetrical coordination spheres and bond lengths (Figure 1). The key point is that a judicious choice of ancillary ligand in conjunction with lead(II) may fine-tune the 6p-character in the 6sp-hybrid orbital, thereby impacting the structure and properties of the resulting coordination polymer.[30,31]

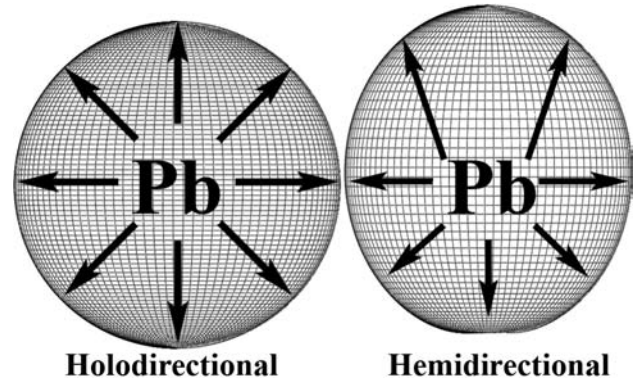

Figure 1. (left) Symmetric bond lengths in a Pb(II) complex with no lone pair activity. (right) Hemidirected bond lengths, shorter lengths away from the lone pair, and longer bond lengths towards the lone pair in a Pb(II) complex with lone pair activity.[29]

To investigate this design concept, we utilized as a reference point our recently reported, highly birefringent $Pb(H_2O)[Au(CN)_2]_2$ coordination polymer, which was also characterized by multinuclear solid-state NMR and featured a hemidirectional lead(II) center.[32] The stereochemically active lone pair played an important role in directing the polymeric structure and influenced the solid-state NMR and birefringent properties of the material. In this current investigation, replacement of the water molecule with a series of nitrogen-donor ancillary ligands having a range of basicities has yielded several coordination polymers in which the degree of the lone pair activity (s/p-hybridization) is purposely modified, thereby altering the overall polymer topology.

To date, the determination of lone pair stereochemical activity in Pb(II) systems has almost exclusively relied on X-ray structural data, as described above.[33–41] However, the

(9) Lin, Z.; Chen, L.; Yue, C.; Yuan, D.; Jiang, F.; Hong, M. *J. Solid State Chem.* **2006**, *179*, 1154.
(10) Maurya, M. R.; Kumar, A. *J. Mol. Cata. A: Chem.* **2006**, *250*, 190.
(11) Steel, P. J. *Acc. Chem. Res.* **2005**, *38*, 243.
(12) Leznoff, D. B.; Xue, B.-Y.; Batchelor, R. J.; Einstein, F. W. B.; Patrick, B. O. *Inorg. Chem.* **2001**, *40*, 6026.
(13) Shorrock, C. J.; Jong, H.; Batchelor, R. J. B. L. D. *Inorg. Chem.* **2003**, *42*, 3917.
(14) Shorrock, C. J.; Xue, B.-Y.; Kim, P. B.; Batchelor, R. J.; Patrick, B. O.; Leznoff, D. B. *Inorg. Chem.* **2002**, *41*, 6743.
(15) Draper, N. D.; Batchelor, R. J.; Leznoff, D. B. *Cryst. Growth Des.* **2004**, *4*, 621.
(16) Lefebvre, J.; Leznoff, D. B. In *Metal and Metalloid-containing Polymers*; Wiley: New York, 2005; Vol. *5*, pp 155−208.
(17) Balboaa, S.; Castiñeirasa, A.; Herleb, P. S.; Strähleb, J. *Z. Anorg. Allg. Chem.* **2007**, *633*, 2420.
(18) Padmanabhan, M.; Joseph, K. C.; Thirumurugan, A.; Huang, X.; Emge, T. J.; Li, J. *Inorg. Chim. Acta* **2007**, *360*, 2583.
(19) Wanga, J.-J. , Yanga, M.-L.; Hua, H.-M. , Xuea, G.-L., Lib, D.-S., Shia, Q.-Z. *Z. Anorg. Allg. Chem.* **2007**, *633*, 341.
(20) Zhou, L.-J.; Wang, Y.-Y.; Zhou, C.-H.; Wang, C.-J.; Shi, Q.-Z.; Peng, S.-M. *Cryst. Growth Des.* **2007**, *7*, 300.
(21) Meng, X.; Song, Y.; Hou, H.; Fan, Y.; Li, G.; Zhu, Y. *Inorg. Chem.* **2003**, *42*, 1306.
(22) Guloy, A. M.; Tang, Z.; Miranda, P. B.; Srdanov, V. I. *Adv. Mater.* **2001**, *13*, 833.
(23) Singh, N. B.; Suhre, D. R.; Green, K.; Fernelius, N.; Hopkins, F. K. *J. Cryst. Growth* **2005**, *274*, 132.
(24) Sui, B.; Zhao, W.; Ma, G.; Okamura, T.-A.; Fan, J.; Li, Y.-Z.; Tang, S.-H.; Sun, W.-Y.; Ueyama, N. *J. Mater. Chem.* **2004**, *14*, 1631.
(25) Mitzi, D. B.; Wang, S.; Feild, C. A.; Chess, C. A.; Guloy, A. M. *Science* **1995**, *267*, 1473.
(26) Kondo, T.; Iwamoto, S.; Hayase, S.; Tanaka, K.; Ishi, J.; Mizuno, M.; Ema, K.; Ito, R. *Solid State Commun.* **1998**, *105*, 503.
(27) Smirnova, E. P.; Aleksandrov, S. E.; Sotnikov, K. A.; Kapralov, A. A.; Sotnikov, A. V. *Phys. Solid State* **2003**, *45*, 1305.
(28) Kagan, C. R.; Mitzi, D. B.; Dimitrakopoulos, C. D. *Science* **1999**, *286*, 945.
(29) Shimoni-Livny, L.; Glusker, J. P.; Bock, C. W. *Inorg. Chem.* **1998**, *37*, 1853.
(30) Davidovich, R. L. *Russ. J. Coord. Chem. (Engl. Transl.)* **2005**, *31*, 445.
(31) Reger, D. L.; Wright, T. D.; Little, C. A.; Lamba, J. J. S.; Smith, M. D. *Inorg. Chem.* **2001**, *40*, 3810.
(32) Katz, M. J.; Aguiar, P. M.; Batchelor, R. J.; Bokov, A. A.; Ye, Z.-G.; Kroeker, S.; Leznoff, D. B. *J. Am. Chem. Soc.* **2006**, *128*, 3669.
(33) Yang, J.; Li, G.-D.; Cao, J.-J.; Yue, Q.; Li, G.-H.; Chen, J.-S. *Chem.—Eur. J.* **2007**, *13*, 3248.
(34) Pellissier, A.; Bretonniere, Y.; Chatterton, N.; Pecaut, J.; Delangle, P.; Mazzanti, M. *Inorg. Chem.* **2007**, *46*, 3714.
(35) Yang, J.; Ma, J.-F.; Liu, Y.-Y.; Ma, J.-C.; Batten, S. R. *Inorg. Chem.* **2007**, *46*, 3542.
(36) Harrowfield, J. M.; Miyamae, H.; Skelton, B. W.; Soudi, A. A.; White, A. H. *Aust. J. Chem.* **1996**, *49*, 1029.
(37) Bytheway, I.; Engelhardt, L. M.; Harrowfield, J. M.; Kepert, D. L.; Miyamae, H.; Patrick, J. M.; Skelton, B. W.; Soudi, A. A.; White, A. H. *Aust. J. Chem.* **1996**, *49*, 1099.
(38) Engelhardt, L. M.; Patrick, J. M.; White, A. H. *Aust. J. Chem.* **1989**, *42*, 335.
(39) Engelhardt, L. M.; Furphy, B. M.; Harrowfield, J. M.; Patrick, J. M.; Skelton, B. W.; White, A. H. *J. Chem. Soc., Dalton Trans.* **1989**, 595.
(40) Engelhardt, L. M.; Harrowfield, J. M.; Miyamae, H.; Patrick, J. M.; Skelton, B. W.; Soudi, A. A.; White, A. H. *Aust. J. Chem.* **1996**, *49*, 1111.

potential utility of spectroscopic methods to observe the status of the lone pair has been relatively neglected. For example, lead-207 NMR is ideal for probing local structure and symmetry in these materials. A reasonably receptive spin-1/2 nucleus, ^{207}Pb has a very large chemical shift range (ca. 16 000 ppm) and is correspondingly sensitive to subtle changes in the local environment about the lead center. In combination with molecular orbital calculations, anisotropic NMR chemical shifts can also provide valuable information about the electronic structure near the nucleus of interest. In the present case, this provides an opportunity to identify nonstructural evidence of lone pair activity, an approach not extensively investigated in the literature.[29,42,43] Similarly, the emission spectra of the polymers was also examined to discern any other nonstructural evidence of lone pair activity.

Experimental Section

General Procedures and Physical Measurements. All manipulations were performed in air. Unless otherwise noted, all reagents, including ligands 1,10-phenanthroline (phen), 2,2′-bipyridine (bipy), and ethylenediamine (en) were obtained from commercial sources and used as received. $[^nBu_4N][Au(CN)_2]\cdot{}^1/_2H_2O$, $[Pb(phen)_2](ClO_4)_2$, and $[Pb(bipy)_2](ClO_4)_2$ were prepared as previously reported,[37,40,44] and their X-ray powder patterns matched the pattern predicted from the reported single crystal data.

Infrared spectra were recorded as KBr pressed pellets on a Thermo Nicolet Nexus 670 FT-IR spectrometer. Raman spectra were acquired with a Thermo Nicolet Nexus 670 FT-Raman equipped with a Nd:YAG laser (1064 nm). Spectra were coadded from a total of 512 scans acquired with a laser power of 100 mW and 1 cm^{-1} instrument resolution. Microanalyses (C, H, N) were performed at Simon Fraser University by Mr. Miki Yang. X-ray powder patterns were collected on a Rigaku RAXIS Rapid curved image plate area detector with graphite monochromator, utilizing Cu Kα radiation. Half-hour scans were taken with a 0.5 μm collimator and a φ spinning speed of 10°/sec, ω was held at 90°, and χ was held at 0°. The powder was adhered to a glass fiber with grease.

Synthetic Procedures. ***Caution!*** *Although we have experienced no difficulties, perchlorate salts are potentially explosive and should only be used in small quantities and handled with care.*

$[Pb(phen)_2][Au(CN)_2]_2$ (1). To a 15 mL methanol/water (1:1) solution containing $Pb(ClO_4)_2\cdot xH_2O$ (40 mg, 0.098 mmol) was added a 15 mL methanol/water (2:1) solution of 1,10-phenanthroline monohydrate (phen, 40 mg, 0.202 mmol). To the resulting solution was then added a 20 mL methanol/water (1:1) solution of $KAu(CN)_2$ (56 mg, 0.194 mmol). Crystals began to form almost immediately. The mixture was allowed to settle overnight, after which it was filtered yielding clear, colorless X-ray quality crystals of $[Pb(phen)_2][Au(CN)_2]_2$ (**1**). Yield: 73 mg (70%). Anal. Calcd for $C_{28}H_{16}N_8Au_2Pb$: C, 31.55%; H, 1.51%; N, 10.51%. Found: C, 31.74%; H, 1.55%; N, 10.38%. IR (KBr, cm^{-1}): 3074, (vw) 2148 (s, νCN), 1620 (w), 1590 (w), 1567 (w), 1514 (s), 1497 (w), 1423 (s), 1346 (w), 1309 (vw), 1212 (vw), 1202 (vw), 1131 (w), 1091 (m), 860 (m), 837 (s) 764 (m), 726 (s), 713 (m), 632 (m). Raman: 2164 cm^{-1} (s, ν_{CN}).

Table 1. Crystallographic Data for **1**, **2**, and **3**

	1	**2**	**3**
empirical formula	$C_{28}H_{16}N_8Au_2Pb$	$C_{24}H_{16}N_8Au_2Pb$	$C_6H_8N_6Au_2Pb$
formula weight	1065.64	1017.60	765.30
crystal system	orthorhombic	monoclinic	monoclinic
space group	*Fddd*	*P2/n*	$P2_1/c$
a, Å	6.9317(13)	10.4838(13)	10.2194(2)
b, Å	20.885(5)	8.8934(7)	11.5000(2)
c, Å	36.459(5)	13.3141(15)	11.2160(3)
α, °	90	90	90
β, °	90	92.777(10)	108.9117(13)
γ, °	90	90	90
V, Å^3	5278.1(18)	1239.9(2)	1246.98(5)
Z	8	2	4
T, K	293	293	100(2)
ρ_{calcd}, g·cm^{-3}	2.682	4.615	4.076
μ, mm^{-1}	17.489	18.605	36.918
R^a, (I > 2.5σ(I))	0.0381	0.0327	0.0415
$R_w{}^a$, (I > 2.5σ(I))	0.0554	0.0319	0.0491
goodness of fit	1.086	1.373	1.067

[a] Function minimized $\Sigma w(||F_o| - |F_c||)^2$ where $w^{-1} = [\sigma^2(F_o) + (nF_o)^2]$, $R = \Sigma||F_o| - |F_c||/\Sigma|F_o|$, $R_w = [\Sigma w(|F_o| - |F_c|)^2/\Sigma w|F_o|^2]^{1/2}$, $n = 0.040$ for **1**, 0.010 for **2**, and 0.030 for **3.**

$[Pb(bipy)_2][Au(CN)_2]_2$ (2). To a 10 mL methanol/water (1:1) solution containing $Pb(ClO_4)_2\cdot xH_2O$ (42 mg, 0.103 mmol) was added a 10 mL methanol/water (1:1) solution of 2,2′-bipyridine (bipy, 30 mg, 0.192 mmol). To the resulting solution was added a 20 mL methanol/water (1:1) solution of $KAu(CN)_2$ (56 mg, 0.194 mmol). The solution initially became cloudy but after 24 h single crystals began to deposit. The solution was allowed to partially, slowly evaporate for a week, after which it was filtered, yielding clear colorless X-ray quality crystals of $[Pb(bipy)_2][Au(CN)_2]_2$ (**2**). Yield: 54 mg (55%). Anal. Calcd for $C_{24}H_{16}N_8Au_2Pb$: C, 28.32%; H, 1.58%; N, 11.01%. Found: C, 28.42%; H, 1.68%; N, 11.17%. IR (KBr, cm^{-1}): 3118 (w), 3106 (w), 3076 (w), 3059 (w), 3041 (w), 2154 (m, νCN), 2140 (s, νCN), 1595 (m), 1576 (m), 1566 (m), 1493 (m), 1475 (m), 1439 (m), 1319 (m), 1244 (m), 1206 (w), 1179 (w), 1156 (m), 1104 (w), 1063 (m), 1040 (w), 1008 (m), 966 (w), 958 (w), 899 (w), 884 (w), 805 (w), 766 (m), 759 (s), 734 (m), 654 (m), 640 (m), 622 (m). Raman: 2155 cm^{-1} (s, ν_{CN}).

$[Pb(en)][Au(CN)_2]_2$ (3). To a 10 mL acetonitrile solution containing $Pb(ClO_4)_2\cdot xH_2O$ (40 mg, 0.098 mmol) was added an acetonitrile solution containing ethylenediamine (en, 1 mL of a 0.1 M stock solution, 0.100 mmol). To the resulting solution was added a 10 mL acetonitrile solution of $[^nBu_4N][Au(CN)_2]\cdot{}^1/_2H_2O$ (100 mg, 0.200 mmol). A precipitate formed immediately. The resulting mixture was allowed to settle overnight, after which it was filtered to obtain microcrystalline $[Pb(en)][Au(CN)_2]_2$ (**3**). Yield: 50 mg (66%). Anal. Calcd for $C_6H_8N_6Au_2Pb$: C, 9.42%; H, 1.05%; N, 10.98%. Found: C, 9.34%; H, 1.02%; N, 10.84%. IR (KBr, cm^{-1}): 3320 (m), 3238 (m), 3209 (m), 3126 (m), 2954 (w), 2932 (w), 2920 (w), 2880 (w), 2866 (w), 2156 (m, νCN), 2143 (s, νCN), 1573 (m), 1309 (w), 1120 (w), 1082 (w), 1053 (w), 1022 (m), 984 (m), 964 (m), 864 (w), 495 (m). Raman: 2172 cm^{-1} (m, ν_{CN}), 2157 cm^{-1} (m, ν_{CN}), 2145 cm^{-1} (w, ν_{CN}). Single crystals of **3** were obtained by altering the Pb/en/Au ratio to 1:1.5:1 and mixing the reagents in 50 mL of acetonitrile, after which the solution was left covered overnight. Small X-ray quality crystals and some powder of **3** were deposited. The crystals had comparable IR and simulated powder X-ray data to the bulk powder.

X-ray Crystallographic Analysis. Crystallographic data for all structures are collected in Table 1. The crystals were mounted on glass fibers using epoxy adhesive. Crystal descriptions for each compound are as follows: **1** was a colorless plate having dimensions 0.40 × 0.40 × 0.02 mm^3; **2** was a colorless block having dimensions 0.28 × 0.14 × 0.11 mm^3; **3** was a colorless block having dimen-

(41) Harrowfield, J. M.; Miyamae, H.; Skelton, B. W.; Soudi, A. A.; White, A. H. *Aust. J. Chem.* **1996**, *49*, 1121.
(42) Walsh, A.; Watson, G. W. *J. Sol. State. Chem.* **2005**, *178*, 1422.
(43) Briand, G. G.; Smith, A. D.; Schatte, G.; Rossini, A. J.; Schurko, R. W. *Inorg. Chem.* **2007**, *46*, 8625.
(44) Lefebvre, J.; Chartrand, D.; Leznoff, D. B. *Polyhedron* **2007**, *26*, 2189.

Table 2. Selected Bond Lengths (Å) and Angles (°) for **1**[a]

Pb(1)−N(1)	2.725(12)	Pb(1)−N(2)	2.722(10)
Pb(1)−N(1")	2.725(12)	Pb(1)−N(2")	2.722(10)
Pb(1)−N(1′)	2.725(12)	Pb(1)−N(2′)	2.722(10)
Pb(1)−N(1*)	2.725(12)	Pb(1)−N(2*)	2.722(10)
Au(1)−C(1)	1.960(18)	C(1)−N(1)	1.15(2)
N(2*)−Pb(1)−N(1)	78.5(3)	N(2′)−Pb(1)−N(1)	73.6(3)
N(2")−Pb(1)−N(1)	78.4(3)	N(1*)−Pb(1)−N(1)	111.6(6)
N(1′)−Pb(1)−N(1)	77.7(6)	N(1")−Pb(1)−N(1)	147.6(5)
N(2′)−Pb(1)−N(2)	150.2(4)	N(2")−Pb(1)−N(2)	60.2(4)
N(1*)−Pb(1)−N(2)	78.5(3)	N(1′)−Pb(1)−N(2)	73.6(4)
N(2*)−Pb(1)−N(2)	129.0(4)	N(1")−Pb(1)−N(2)	78.4(3)
N(1)−Pb(1)−N(2)	133.1(3)	N(2*)−Pb(1)−N(2′)	60.2(4)
N(2*)−Pb(1)−N(2")	150.2(4)	N(2′)−Pb(1)−N(2")	129.0(4)
N(2*)−Pb(1)−N(1*)	133.1(3)	N(2′)−Pb(1)−N(1*)	78.4(3)
N(2")−Pb(1)−N(1*)	73.6(3)	N(2*)−Pb(1)−N(1′)	78.4(3)
N(2′)−Pb(1)−N(1′)	133.1(3)	N(2")−Pb(1)−N(1′)	78.5(3)
N(1*)−Pb(1)−N(1′)	147.6(5)	N(2*)−Pb(1)−N(1")	73.6(3)
N(2′)−Pb(1)−N(1")	78.5(3)	N(2")−Pb(1)−N(1")	133.1(3)
N(1*)−Pb(1)−N(1")	77.7(6)	N(1′)−Pb(1)−N(1")	111.6(6)
Pb(1)−N(1)−C(1)	144.3(12)		

[a] Symmetry transformations: ": $-x + 5/4, -y + 1/4, z$; *: $x, -y + 1/4, -z + 1/4$; ′: $-x + 5/4, y, -z + 1/4$.

sions 0.11 × 0.08 × 0.06 mm^3. The data for **1** and **2** were collected at room temperature using the diffractometer control program DIFRAC[45] and an Enraf Nonius CAD4F diffractometer with Mo Kα radiation. The following data ranges were recorded: **1** = 4° ≤ 2θ ≤ 60°; **2** = 4° ≤ 2θ ≤ 50°. The data were corrected by integration for the effects of absorption using a semiempirical psi-scan method with the following transmission ranges: **1** = 0.042 − 0.196; **2** = 0.036 − 0.101. Data reduction included corrections for Lorentz and polarization effects. Final unit-cell dimensions were determined based on the following well-centered reflections: **1** = 40 reflections with range 40° ≤ 2θ ≤ 44°; **2** = 42 reflections with range 30° ≤ 2θ ≤ 32°.

The data for **3** were measured at 100 ± 2 K on a Bruker Kappa APEX I CCD area detector system equipped with a graphite monochromator and a Mo Kα sealed tube. The detector was placed at a distance of 2.5 cm from the crystal. A total of 210 frames were collected with a scan width of 2.0° in ω and an exposure time of 120 s/frame. The total data collection time was 7 h. Data were corrected for absorption effects using the numerical face-indexed technique (SADABS). The calculated minimum and maximum transmission coefficients (based on crystal size) are 0.017 and 0.109.

For all three compounds, coordinates and anisotropic displacement parameters for the non-hydrogen atoms were refined, with the exception of the ethylenediamine carbon atoms, which were found to be disordered in two conformations and consequently refined isotropically. Hydrogen atoms were placed in calculated positions (*d* C−H 0.93−0.95 Å, *d* N−H 0.86−0.89 Å) and initially refined with soft restraints on the bond lengths and angles to regularize their geometry; afterward, their coordinate shifts were linked with those of the respective carbon or nitrogen atoms during refinement. Isotropic thermal parameters for the hydrogen atoms were initially assigned proportionately to the equivalent isotropic thermal parameters of their respective carbon or nitrogen atoms. Subsequently, the isotropic thermal parameters for the C−H or N−H hydrogen atoms were constrained to have identical shifts during refinement. Selected bond lengths and angles for **1**−**3** are found in Tables 2–4.

The programs used for all absorption corrections, data reduction, and processing for **1** and **2** were from the NRCVAX[46] Crystal Structure System; for **3**, the Bruker SAINT software package was used. All structures were solved using Sir 92, expanded using

Table 3. Selected Bond Lengths (Å) and Angles (°) for **2**[a]

Pb(1)−N(1*)	3.091(13)	Pb(1)−N(1′)	3.091(13)
Pb(1)−N(2)	2.912(13)	Pb(1)−N(2")	2.912(13)
Pb(1)−N(3)	2.597(10)	Pb(1)−N(3")	2.597(10)
Pb(1)−N(4)	2.629(9)	Pb(1)−N(4")	2.629(9)
Au(1)−Au(1′)	3.5925(11)	Au(1)−C(1)	1.964(15)
Au(1)−C(2)	1.969(16)	C(1)−N(1)	1.135(16)
C(2)−N(2)	1.130(16)		
N(3")−Pb(1)−N(4")	62.0(3)	N(3")−Pb(1)−N(3)	75.6(4)
N(4")−Pb(1)−N(3)	79.4(3)	N(3")−Pb(1)−N(4)	79.4(3)
N(4")−Pb(1)−N(4)	131.1(4)	N(3)−Pb(1)−N(4)	62.0(3)
N(3")−Pb(1)−N(2)	74.4(3)	N(4")−Pb(1)−N(2)	113.9(3)
N(3)−Pb(1)−N(2)	134.8(3)	N(4)−Pb(1)−N(2)	79.8(3)
N(3")−Pb(1)−N(2")	134.8(3)	N(4")−Pb(1)−N(2")	79.8(3)
N(3)−Pb(1)−N(2")	74.4(3)	N(4)−Pb(1)−N(2")	113.9(3)
N(2)−Pb(1)−N(2")	148.0(5)	N(3")−Pb(1)−N(1′)	139.7(3)
N(4")−Pb(1)−N(1′)	155.3(3)	N(3)−Pb(1)−N(1′)	113.9(3)
N(4)−Pb(1)−N(1′)	72.7(3)	N(2)−Pb(1)−N(1′)	72.5(3)
N(3")−Pb(1)−N(1*)	113.9(3)	N(4")−Pb(1)−N(1*)	72.7(3)
N(3)−Pb(1)−N(1*)	139.7(3)	N(4)−Pb(1)−N(1*)	155.3(3)
N(2)−Pb(1)−N(1*)	83.9(3)	N(2")−Pb(1)−N(1′)	83.9(3)
N(2")−Pb(1)−N(1*)	72.5(3)	N(1′)−Pb(1)−N(1*)	84.7(4)
C(1)−N(1)−Pb(1′)	132.1(10)	C(2)−N(2)−Pb(1)	156.4(11)

[a] Symmetry transformations: ′: $-x + 1, -y + 4, -z + 2$; ": $-x + 1/2, y, -z + 5/2$; *: $x - 1/2, -y + 4, z + 1/2$.

Table 4. Selected Bond Lengths (Å) and Angles (°) for **3**[a]

Pb(1)−N(1)	2.624(8)	Pb(1)−N(2")	2.887(9)
Pb(1)−N(3)	3.035(9)	Pb(1)−N(5)	2.123(7)
Pb(1)−N(6)	2.488(9)	Pb(1)−Au(1*)	3.5494(5)
Au(1)−Au(2′)	3.3798(5)	Au(1)−Au(2[†])	3.3221(5)
Au(2)−Au(2[‡])	3.2495(7)	Au(1)−C(1)	2.057(10)
Au(1)−C(2)	2.068(10)	Au(2)−C(3)	2.274(12)
Au(2)−C(4)	2.282(11)		
N(2")−Pb(1)−N(1)	81.6(3)	N(2")−Pb(1)−N(5)	73.5(3)
N(1)−Pb(1)−N(5)	86.3(3)	N(2")−Pb(1)−N(6)	146.1(2)
N(1)−Pb(1)−N(6)	91.6(3)	N(5)−Pb(1)−N(6)	73.0(3)
N(2")−Pb(1)−N(3)	104.1(3)	N(1)−Pb(1)−N(3)	156.4(3)
N(5)−Pb(1)−N(3)	73.8(3)	N(6)−Pb(1)−N(3)	70.8(3)
N(2′)−Pb(1)−Au(1*)	73.60(17)	N(1)−Pb(1)−Au(1*)	74.69(18)
N(5)−Pb(1)−Au(1*)	143.9(2)	N(6)−Pb(1)−Au(1*)	136.5(2)
N(3)−Pb(1)−Au(1*)	128.93(18)	Au(2′)−Au(1)−Au(2[†])	162.156(13)
Pb(1[§])−Au(1)−Au(2[†])	86.015(11)	Au(2[‡])−Au(2)−Au(1[§])	87.182(14)
Pb(1)−N(1)−C(1)	174.2(7)	Pb(1)−N(2")−C(2")	143.3(7)
C(3)−N(3)−Pb(1)	163.7(8)		

[a] Symmetry transformations: ′: $-x + 1, y + 1/2, -z + 1/2$; ": $-x, y - 1/2, -z - 1/2$; *: $x, -y + 3/2, z + 1/2$; [†]: $x - 1, y, z$; [‡]: $-x + 2, -y + 1, -z + 1$; [§]: $-x + 1, y - 1/2, -z + 1/2$; [§]: $x, -y + 3/2, z - 1/2$.

Fourier techniques and refined using CRYSTALS.[47] Complex scattering factors for neutral atoms were used in the calculation of structure factors. Diagrams were made using ORTEP-3,[48] POV-RAY,[49] and Cameron.[50]

Nuclear Magnetic Resonance Spectroscopy. ^{207}Pb MAS NMR was done on a Varian Inova 600 (B_o = 14.1 T) at 125.08 MHz, using a 5.0 mm double-resonance magic-angle spinning probe (Varian-Chemagnetics) with spinning speeds of 6000 ± 1 to 11400 ± 3 Hz. Single-pulse experiments with a 0.8 μs excitation pulse (tip angle of 15°) were used, with 5 s relaxation delays. Chemical shifts are reported with respect to $Pb(CH_3)_4$ using 1.0 M lead nitrate

(45) Gabe, E. J.; White, P. S.; Enright, G. D. *DIFRAC: A Fortran 77 Control Routine for 4-Circle Diffractometers*; N. R. C.: Ottawa, 1995.
(46) Gabe, E. J.; Page, Y. L.; Charland, J. P.; Lee, F. L.; White, P. S. *J. Appl. Crystallogr.* **1989**, *22*, 384.
(47) Betteridge, P. W.; Carruthers, J. R.; Cooper, R. I.; Prout, K.; Watkin, D. J. *J. Appl. Crystallogr.* **2003**, *36*, 1487.
(48) Farrugia, L. J. *J. Appl. Crystallogr.* **1997**, *30*, 565.
(49) Fenn, T. D.; Ringe, D.; Petsko, G. A. *J. Appl. Crystallogr.* **2003**, *36*, 944; Persistence of Vision Raytracing: http://www.povray.org.
(50) Watkin, D. J.; Prout, C. K.; Pearce, L. J. , *Chemical Crystallography Laboratory*; University of Oxford: Oxford, U.K., 1996.

(−2961.2 ppm) as a secondary reference.[51] Isotropic chemical shifts were identified by comparison of spectra acquired at different spinning rates. Because of the inherent nature of lead chemical shifts being sensitive to changes in temperature, all acquired spectra were maintained at 298 K. Spectra were simulated using STARS, as implemented within VnmrJ (Varian Inc.). The bandwidth of the probe was found to be about 500 kHz ($Q \approx 200$); however, inclusion of this factor in spectral simulations influenced only the compound with the largest chemical shift anisotropy.

Luminescence Measurements. Steady-state photoluminescence spectra were collected using a Photon Technology International Model QuantaMaster-1046 spectrophotometer equipped with a 75 W xenon lamp. Wavelengths were selected with two excitation monochromators and a single emission monochromator. The instrument is interfaced with a computer, and software supplied by the manufacturer was used to collect and record data. Excitation and emission spectra are uncorrected. Powder and/or crystal samples were mounted on a copper plate, and the luminescence spectra were recorded as a function of temperature using liquid nitrogen as the coolant in a Model LT-3−110 Heli-Tran cryogenic liquid transfer system equipped with a temperature controller.

DFT Calculation of Lead Shieldings. Calculations were performed on representative clusters of the three compounds using the Amsterdam Density Functional (ADF) package (version ADF2006−01)[52,53] and accounted for relativistic effects using the spin−orbit method of ZORA (zeroth-order relativistic approximation).[54–58] The GGA functionals of Becke[59] and Perdew[60,61] were used with a double-ζ (DZ) basis set. The calculated shieldings were converted to shifts using the calculated shieldings, at the same level of theory, for tetramethyllead, $Pb(CH_3)_4$.

DFT Calculations of Molecular Orbitals. The molecular structures used in this set of calculations were taken from the X-ray diffraction results. Keeping all distances, angles, and dihedral angles frozen, single-point density functional theory (DFT) ground-state calculations were performed on the models using the Becke three-parameter hybrid exchange functional[62] and the Lee−Yang−Parr correlation functional[63,64] (B3LYP) as implemented in Gaussian 03.[65] In the calculations, the Dunning/Huzinaga valence double-ζ[66] (DV95) basis sets were used for C, N, and H, while the Stuttgart/Dresden effective core potentials were used for Au and Pb.[67,68] Graphical representation of the highest occupied molecular orbital (HOMO) and lowest unoccupied molecular orbital (LUMO) were generated using Gabedit,[69] and population analyses were performed using PyMOlyze.[70]

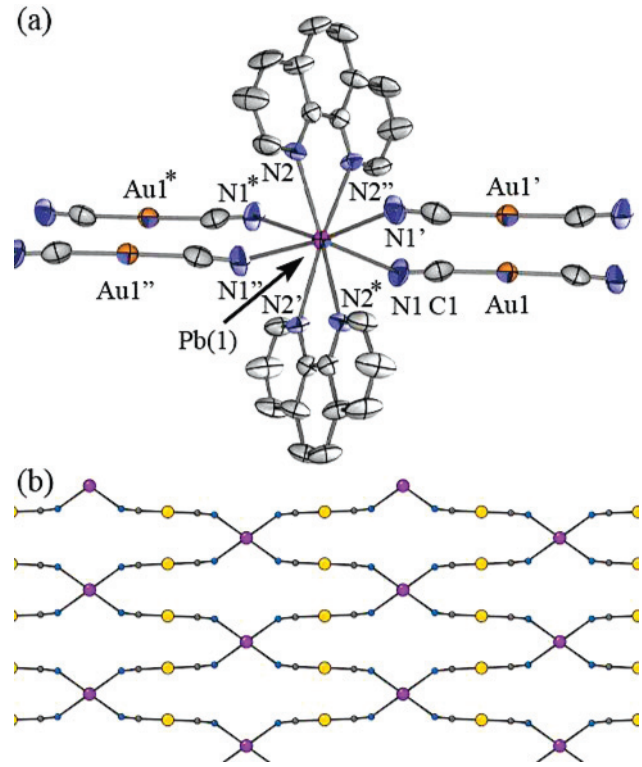

Figure 2. (a) Local site geometry about the Pb(II) center of **1**. (b) 2-D brick-wall structure of **1** viewed down the *c*-axis. Phenanthroline ligands removed for clarity.

Results and Discussion

Structure of $[Pb(phen)_2][Au(CN)_2]_2$ (1). The structure of **1** contains an eight-coordinate distorted square-antiprismatic Pb(II) center with nonpolar point group D_2 symmetry. The Pb(II) coordination sphere contains two trans phenanthroline ligands, with the remaining four sites occupied by two sets of N-bound cyanides, which are also trans to each other (Figure 2a). The dihedral angle between the two planar phen ligands is 30.0°, indicating a propeller-like orientation around the Pb(II). The Pb−N bond lengths in **1** are all 2.72 Å, indicating that the lead(II) center is holodirectional, showing no crystallographic evidence for a stereochemically active lone pair. The lead coordination sphere observed in **1** can be compared to that found for the $[Pb(phen)_2(oxalate)]\cdot 5H_2O$ coordination polymer, which also has Pb−N and Pb−O bond lengths of 2.721(2) and 2.704(2); that is, the lone pair was also found to be stereochemically inactive.[71] However, lead(II)-$phen_2$ complexes in which the presence of the lone pair is evident, such as $[Pb(phen)_2](ClO_4)_2$, show a noticeable variation in Pb−N(phen) bond lengths, ranging from 2.41(2) to 2.73(1) Å, all equivalent or below the

(51) Maciel, G. E.; Dallas, J. L. *J. Am. Chem. Soc.* **1973**, *95*, 3039.
(52) Fonseca Guerra, C.; Snijders, J. G.; te Velde, G.; Baerends, E. J. *Theor. Chem. Acc.* **1998**, *99*, 391.
(53) *ADF 2006.01, SCM*; Theoretical Chemistry, Vrije Universiteit: Amsterdam, The Netherlands, 2006; http://www.scm.com.
(54) Schreckenbach, G.; Ziegler, T. *J. Phys. Chem.* **1995**, *99*, 606.
(55) Schreckenbach, G.; Ziegler, T. *Int. J. Quantum Chem.* **1996**, *60*, 753.
(56) Schreckenbach, G.; Ziegler, T. *Int. J. Quantum Chem.* **1997**, *61*, 899.
(57) Wolff, S. K.; Ziegler, T. *J. Phys. Chem.* **1998**, *109*, 895.
(58) Wolff, S. K.; Ziegler, T.; van Lenthe, E.; Baerends, E. J. *J. Chem. Phys.* **1999**, *110*, 7689.
(59) Becke, A. D. *Phys. Rev. A* **1988**, *38*, 3098.
(60) Perdew, J. P. *Phys. Rev. B: Condens. Matter* **1986**, *33*, 8822.
(61) Perdew, J. P. *Phys. Rev. B: Condens. Matter* **1986**, *34*, 7406.
(62) Becke, A. D. *J. Chem. Phys.* **1993**, *98*, 5648.
(63) Lee, C.; Yang, W.; Parr, R. G. *Phys. Rev. B: Condens. Matter* **1988**, *37*, 785.
(64) Miehlich, B.; Savin, A.; Stoll, H.; Preuss, H. *Chem. Phys. Lett.* **1989**, *157*, 200.
(65) Frisch, M. J. et al., *Gaussian 03* Revision C2; Gaussian, Inc.: Wallingford, CT, 2004.
(66) Dunning, T. H., Jr., Hay, P. J. In *Modern Theoretical Chemistry*; Schaefer, H. F., III, Ed.; Plenum: New York, 1976; pp 1−28.
(67) Dolg, M.; Stoll, H.; Preuss, H.; Pitzer, R. M. *J. Phys. Chem.* **1993**, *97*, 5852.
(68) Kuechle, W.; Dolg, M.; Stoll, H.; Preuss, H. *Mol. Phys.* **1991**, *74*, 1245.
(69) Allouche, A. R. *Gabedit* [online] version 2.0.9; http://gabedit.sourceforge.net/ (accessed February 2007).
(70) Tenderholt, A. L. *PyMOlyze* [online], version 2.0; http://pymolyze.sourceforge.net (accessed April 2007).
(71) Zhu, L.-H.; Zeng, M.-H.; Ye, B.-H.; Chen, X.-M. *Z. Anorg. Allg. Chem.* **2004**, *630*, 952.

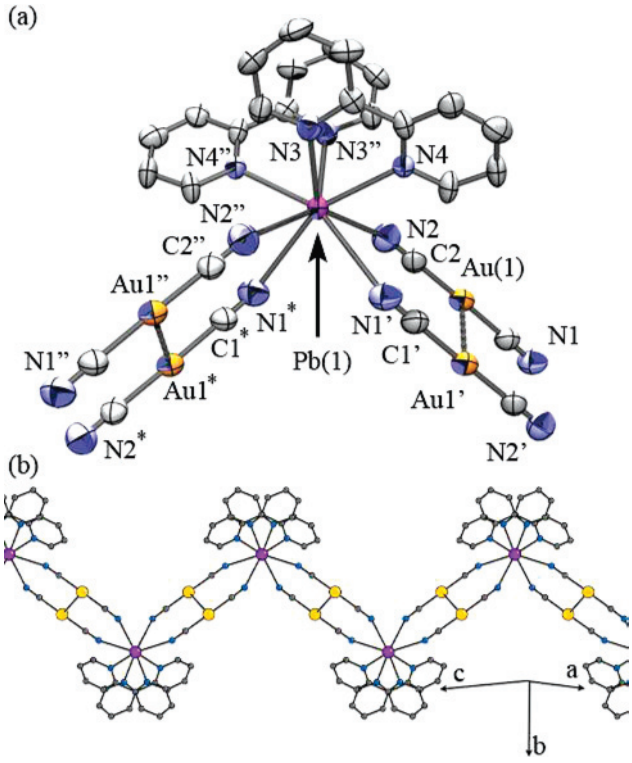

Figure 3. (a) Local site geometry about the Pb(II) center of **2**. (b) Extended 1-D chain structure of **2**.

2.72 Å seen here.[37–39] Interestingly, among the other known $[Pb(phen)_2]^{2+}$-containing structures,[72] the oxalate polymer and **1** are the only ones which are holodirectional.

While the bridging oxalate in $[Pb(phen)_2(oxalate)]\cdot 5H_2O$ generates a 1-D chain, in **1** each of the four $[Au(CN)_2]$-units on a given Pb(II) center binds to a different Pb(II) with its other cyano group, thereby forming a 2-D (4,4)-network structure (Figure 2b).[73] The sheets stack upon one another via weak $\pi-\pi$ interactions of 3.58(3) Å. This is significantly longer than the 3.25 Å $\pi-\pi$ stacking observed in the related oxalate polymer. There are no Au−Au interactions observed in **1**; the shortest distance of Au1−Au1′ = 3.7081(7) Å is longer than the sum of the van der Waals radii of 3.6 Å for two gold(I) centers.[74]

Structure of $[Pb(bipy)_2][Au(CN)_2]_2$ (2). The structure of **2** contains an eight-coordinate distorted square antiprism lead(II) center in the polar point group C_2 in which there are two bipyridine (bipy) units cis to one another, with Pb(1)−N(3) and Pb(1)−N(4) bond lengths of 2.597(10) Å and 2.629(9) Å respectively; the Pb−N bond lengths in known lead(II)-$bipy_2$ complexes range from 2.467(4) to 2.694(6) Å.[40] As in **1**, the remaining four sites on the Pb(II) center are occupied by N-bound cyanides from the linear $[Au(CN)_2]$-units (Figure 3a). However, the Pb(1)−N-cyano bond lengths of Pb(1)−N(1) = 3.091(13) Å and Pb(1)−N(2) = 2.912(13) Å are substantially longer than those observed in **1**, indicating a hemidirectional coordination sphere for **2**. Because of the active stereochemical lone pair, the Pb(II) center in **2** has a dipole. Each pair of cis-cyanoaurate units links to an adjacent lead(II) center, thereby forming a corrugated 1-D chain in which the bipy units always occupy the periphery of the corrugation (Figure 3b). The shortest Au−Au distance in **2** of Au1−Au1′ = 3.5925(11) Å occurs within each chain (Figure 3 dashed lines). The chains further stack via weak $\pi-\pi$ interactions of 3.441(16) Å from the bipy units.

Structure of $[Pb(en)][Au(CN)_2]_2$ (3). The topological structure of **3** is the most complex of the three polymers. In the polar point group C_1, the equatorial plane of the lead(II) is defined by one ethylenediamine unit, having distances of Pb(1)−N(5) = 2.123(7) Å and Pb(1)−N(6) = 2.488(9). The observed en−Pb bond lengths are remarkably asymmetric relative to those found in other $[Pb(en)]^{2+}$ units, for example, 2.429(6) and 2.444(6) Å in $Pb(en)(NO_3)_2$,[36] and 2.397(6) and 2.402(6) Å in the $[NaPb(en)(ClO_4)(NO_3)_2]_n$ polymer.[75] A single N-bound cyanide resides in this plane as well, with Pb(1)−N(2) = 2.887(9) Å. The remaining 60% of this plane contains no short contacts to any nitrogen donors but instead has a ligand-unsupported Pb−Au interaction of 3.5494(5) Å. This is a longer contact than the ligand-supported Pb−Au interactions of 2.896(1) and 2.963(2) Å previously reported[76] but is within the sum of the Pb and Au van der Waals radii.[77] In the axial positions, Pb(1) contains N-bound cyanides with bond lengths of 2.624(8) and 3.035(9) Å for Pb(1)−N(1) and Pb(1)−N(3) (Figure 4a). The N-cyano N(4)−Pb(1) distance of 3.177(9) Å is significantly above the longest reported nitrogen−lead(II) bond of 3.092(6).[41]

Via coordination bonds, the structure of **3** is a 1D zigzag chain having terminal $[Au(CN)_2]^-$ units (Figure 4b). Unlike in **1** and **2**, the chains in **3** are not loosely packed but are held together via gold−gold interactions of 3.2495(7) Å that form a ladder-rung motif, generating an overall 2D sheet similar to the $[Cu(tmeda)][Au(CN)_2]_2$ polymer previously reported (tmeda = *N*,*N*,*N*′,*N*′-tetramethylethylenediamine).[78] Aurophilic interactions of 3.3221(5) and 3.3798(5) Å hold neighboring sheets to one another (not shown). The aforementioned Pb−Au interaction also assists in the sheet stacking.

The three compounds presented herein demonstrate the ability of the ancillary ligand to tune the electron density on the lead(II) center and thus alter the degree to which the stereochemical lone pair is prevalent: in the case of the phen-containing system, **1**, the stereochemical lone pair is completely deactivated. As expected, the most basic ligand, ethylenediamine (pK_a's of 6.848 and 9.928 [79–81]) has the most

(72) Allen, F. H. *Acta Crystallogr.* **2002**, *B58*, 380.
(73) Wells, A. F. *Three-dimensional nets and polyhedra*; John Wiley & Sons: New York, 1977.
(74) Bardaji, M.; Laguna, A. *J. Chem. Educ.* **1999**, *76*, 201.
(75) Morsali, A.; Chen, X.-M. *Helv. Chim. Acta* **2004**, *87*, 3050.
(76) Wang, S.; Garzbn, G.; King, C.; Wang, J.-C.; Fackler, J. P., Jr *Inorg. Chem.* **1989**, *28*, 4623.
(77) Bondi, A. *J. Phys. Chem.* **1964**, *68*, 441.
(78) Leznoff, D. B.; Xue, B.-Y.; Patrick, B. O.; Sanchez, V.; Thompson, R. C. *Chem. Commun.* **2001**, 259.
(79) Harris, D. C. *Exploring Chemical Analysis*, 3rd ed.; W. H. Freeman and Company: New York, 2005.
(80) Perrin, D. D. *Aust. J. Chem.* **1964**, *17*, 484.
(81) Khan, M. N.; Zrifin, Z.; George, A.; Wahab, I. A. *Int. J. Chem. Kinet.* **1999**, *32*, 146.

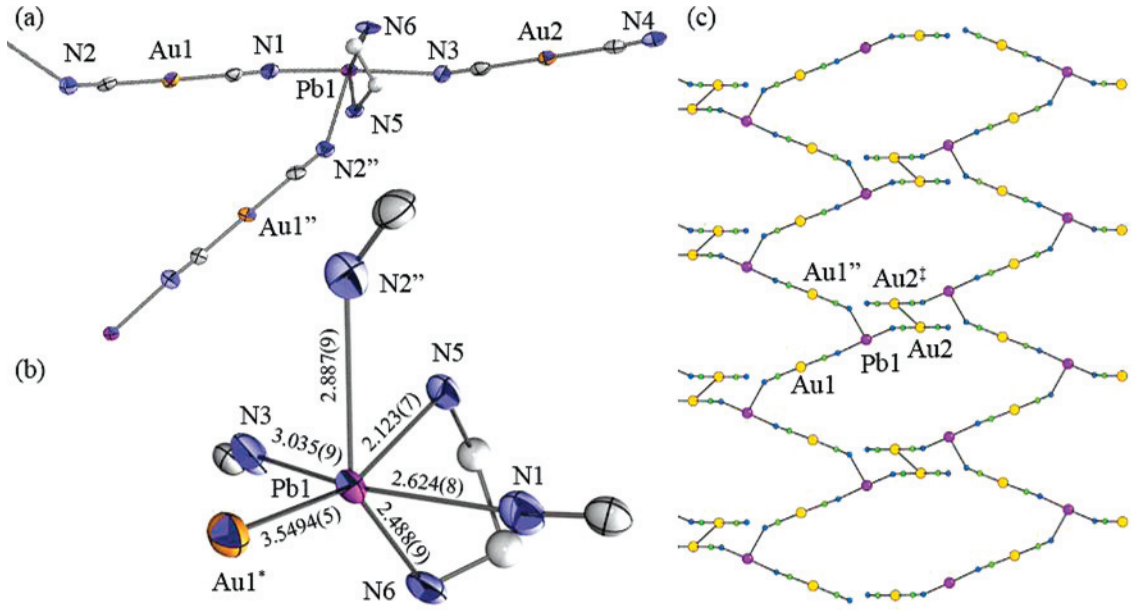

Figure 4. (a) 1-D chain structure of **3**. (b) Local site geometry about the Pb(II) center of **3**. (c) Extended 2-D chain structure of **3** viewed down the *a*-axis. The ethylenediamine unit has been removed for clarity.

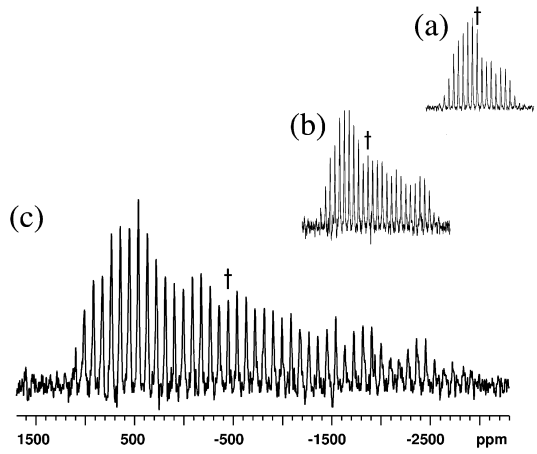

Figure 5. ^{207}Pb MAS spectra of the (a) phenanthroline (**1**), (b) bipyridine (**2**), and (c) ethylenediamine (**3**)-containing polymers. Isotropic chemical shifts are indicated by crosses.

pronounced effect on the lone pair, as evidenced by a low coordination number about the lead (only one en ligand binds) as well as the lowest point group symmetry, C_1.

In the case of the phenanthroline and bipyridine complexes, **1** and **2**, respectively, both complexes have eight-coordinate lead(II), with **1** having more symmetric bond lengths than **2**. The point-symmetry of the lead(II) is also lower in **2** than in **1**, C_2 vs D_2. Consistent with the comparison of basicity and lone pair activity, phenanthroline, having pK_a values of 1.8 and 4.91 for the dication, is less basic than the bipyridine cation with its pK_a of 4.34.[79,80,82]

NMR Spectroscopy. In an effort to establish alternate probes of lead(II) lone pair stereochemical activity, ^{207}Pb MAS NMR spectra of the solid coordination polymers were obtained. The data reveal several structurally informative trends. Figure 5 displays the spectra of compounds **1**, **2**, and **3** plotted on the same scale. As with many cations, ^{207}Pb isotropic chemical shifts have been shown to increase for certain systems as the coordination number decreases,[83] and these data conform to the documented trend (Table 5). However, it is clear that other effects also have a strong influence on the isotropic shifts, since the 8-fold coordinate lead sites in compounds **1** and **2** differ in δ_{iso} by over 1000 ppm. For a given coordination number, a decrease in the size of the cation's coordination sphere has also been found to correlate with increasing isotropic chemical shift.[84] While the *mean* Pb−N bond distances (2.724 ± 0.012 Å for **1**, 2.807 ± 0.41 Å for **2**) do not bear out this generalization, it is worth noting that **1** has a relatively uniform coordination sphere, with bond lengths ranging narrowly from 2.722 to 2.725 Å (see Table 2), whereas **2** possesses a wide range of Pb−N bond lengths from 2.597 to 3.091 Å, thereby defining an irregular polyhedron with some very short contacts which might be responsible for the observed deshielding.

More informative are the individual tensor components, δ_{11}, δ_{22}, and δ_{33}, which represent chemical shielding in different directions within the molecular frame of reference. These components, and their associated parameters, Ω and κ, are known to be more sensitive to the local electronic structure and symmetry than the isotropic averages. Figure 5 clearly illustrates that the dramatic increase in overall shielding span from 740 to 3980 ppm reflects the reduction of symmetry at the lead site, with the least symmetric compound, **3**, possessing the most anisotropic shielding tensor. This exquisite sensitivity to local site symmetry also influences the isotropic chemical shift derived therefrom.

A full characterization of the shielding data necessitates knowledge of the orientation of the shielding principal axis system relative to the molecular geometry. While this can be difficult to reliably obtain with precision, point-group

(82) Beattie, I. R.; Webster, M. *J. Phys. Chem.* **1962**, *66*, 115.

(83) Mackenzie, K. J. D.; Smith, M. E. *Multinuclear Solid-State NMR of Inorganic Materials*; Pergamon: London, 2002.

(84) Kye, Y.-S.; Connolly, S.; Herreros, B.; Harbison, G. S. *Main Group Metal Comp.* **1999**, *22*, 373.

Table 5. ^{207}Pb NMR Parameters for the Lead(ligand)$_x$ Cyanoaurate Polymers **1**−**3**

Pb(ligand)$_x$ cation	δ_{iso} (ppm)	δ_{11} (ppm)	δ_{22} (ppm)	δ_{33} (ppm)	Ω^a (ppm)	κ^b (ppm)
1 Pb(phen)$_2$ EXP	−2970 ± 16	−2645 ± 15	−2891 ± 15	−3383 ± 18	740 ± 32	0.3 ± 0.1
DFT	−1587.9	−1813.4	−1942.0	−1778.1	363.1	−0.29
2 Pb(bipy)$_2$ EXP	−1869 ± 17	−1396 ± 15	−1641 ± 15	−2569 ± 20	1173 ± 35	0.6 ± 0.1
DFT	−1046.5	−1444.1	−1853.9	−1448.2	807.4	0.01
3 Pb(en) EXP	−448 ± 48	1083 ± 40	470 ± 40	−2898 ± 65	3980 ± 105	0.7 ± 0.1
DFT	163.3	−461.8	−1573.4	−624.0	1736.7	0.28

^{a} Span - $\Omega = \delta_{11}$-δ_{33}. ^{b} Skew - $\kappa = 3(\delta_{22} - \delta_{iso})/\Omega$.

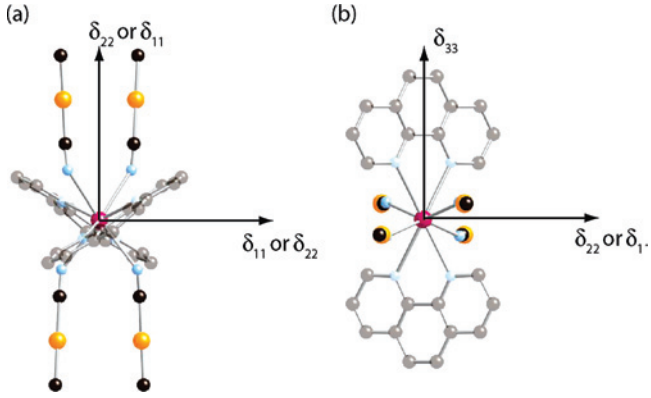

Figure 6. Predicted tensor orientations for Pb(phen)$_2$[Au(CN)$_2$]$_2$ (**1**), shown (a) looking at $hkl = 101$ and (b) $hkl = 010$. The δ_{33} component bisects the phenanthroline ligand, whereas δ_{11} and δ_{22} lie in the pseudoplane formed by the cyanide chains.

symmetry and local bonding considerations can be used to limit the possibilities. In **1**, the Pb(II) cation is located at a site of D_2 point symmetry; thus, three orthogonal C_2 axes converge at that site. The presence of these symmetry elements constrains the orientation of the shielding tensor principal axis system such that the principal components must lie along C_2 axes. One of these rotation axes bisects the phenanthroline rings, and two lie within the pseudoplane formed by the NC−Au−CN chains. Combining these symmetry constraints with the structural environments about each of these rotation axes, a reasonable prediction of the tensor orientation places the similar δ_{11} and δ_{22} components in the cyanide plane, leaving the δ_{33} component along the phenanthroline ligands (Figure 6).

Complex **2** possesses a single C_2 along the *b*-axis on which one of the components must lie. This axis falls between the two symmetry-related bipyridine ligands, offset from the bisectors of the rings (approximately along the arrow in Figure 3a). While the other two shielding components must lie orthogonal to this axis, no additional structural information exists to constrain their orientation within the plane. Given the similar environments of these components, it is likely that they are the δ_{11} and δ_{22} components, such that the unique component (δ_{33}) is directed along the rotation axis.

The lead cation in **3** has C_1 site symmetry and thus lacks any symmetry basis for constraining the orientation of the shielding tensor. However, it may be noted that the δ_{33} component is similar in magnitude to those of **1** and **2**, possibly suggesting that it is directed toward the ethylenediamine ligand, while the δ_{11} and δ_{22} components are significantly deshielded, underscoring the vast differences in their local environments vis-à-vis **1** and **2**. In fact, Figure 7a,b illustrates that the δ_{33} component changes little while the δ_{11} and δ_{22} components become progressively more deshielded (i.e., move to higher frequency) as the lone pair activity increases.

Lacking experimental data or symmetry arguments, theoretical calculations can provide guidance about the orientation of tensor principal components. DFT calculations of the NMR shielding tensor components are in poor agreement with those observed experimentally (Table 5) but nicely mirror the *relative* changes in the individual tensor components among the three compounds. Figure 7 illustrates that both the experimental and calculated tensors change most in the magnitudes of the δ_{11} and δ_{22} components, with consequent increases in the Ω and δ_{iso}. The δ_{33} component exhibits the smallest change among the three compounds investigated, indicating some electronic/structural similarity among the three complexes in the general direction of this component of the shielding tensor. Analysis of the tensor orientations predicted by DFT reveals that the δ_{33} components are not aligned with a particular Pb−N bond. Instead, the hemidirectional complexes **2** and **3** have this component directed into the "gap" in the lead coordination sphere, where the stereochemical lone pair is thought to reside. Similar orientations were found by DFT for a series of lead(II) thiolates, all with highly anisotropic shielding tensors ($\Omega \geq$ 3900 ppm).[43] In the present case, the much larger range of shielding anisotropies and correlation with the degree of stereochemical lone pair activity implies a close link with electronic structure. Indeed, Figure 8 shows that the Mulliken populations calculated for the lead atom have increasing p-character in the following order: **1** < **2** < **3**, reflecting the increasing ^{207}Pb shielding anisotropies.

Luminescence Spectra. Compounds containing d^{10}−d^{10} metallophilic interactions are well-known to have rich luminescence behavior.[85,86] It was thus of interest to examine the excitation and emission spectra of **1**−**3** in terms of attempting to correlate the results with their metallophilic d^{10}−d^{10} or d^{10}−$d^{10}s^2$ interactions[87,88] and to perhaps identify spectroscopic features attributable to the stereochemical activity of the lead(II) lone pair.

The luminescence spectrum of **1** at 77 K shows a broad, featureless peak at 520 nm (Figure 9-black) with excitation maxima at 325 and 340 nm. To assist in assigning the

(85) Stender, M.; White-Morris, R. L.; Olmstead, M. M.; Balch, A. L. *Inorg. Chem.* **2003**, *42*, 4504.
(86) Assefa, Z.; Omary, M. A.; McBurnett, B. G.; Mohamed, A. A.; Patterson, H. H.; Staples, R. J.; Fackler, J. P. *Inorg. Chem.* **2002**, *41*, 6274.
(87) Rawashdeh-Omary, M. A.; Omary, M. A.; Patterson, H. H. *J. Am. Chem. Soc.* **2000**, *122*, 10371.
(88) Rawashdeh-; Omary, M. A.; Omary, M. A.; Patterson, H. H.; Fackler, J. P., Jr *J. Am. Chem. Soc.* **2001**, *123*, 11237.

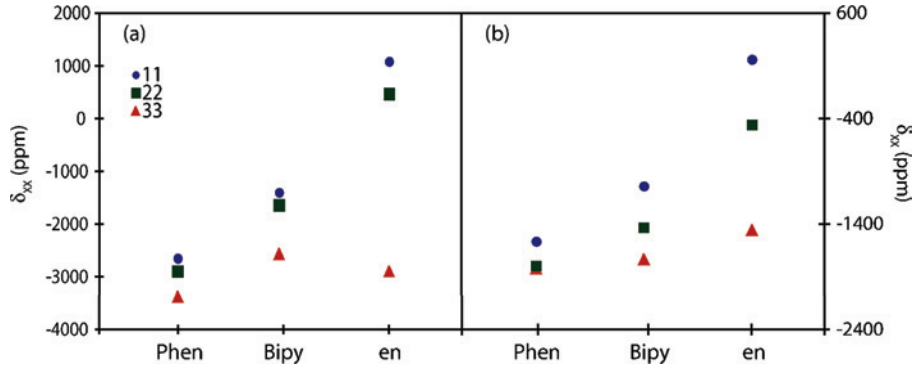

Figure 7. Chemical shift tensor principal components observed (a) experimentally and (b) from DFT calculations.

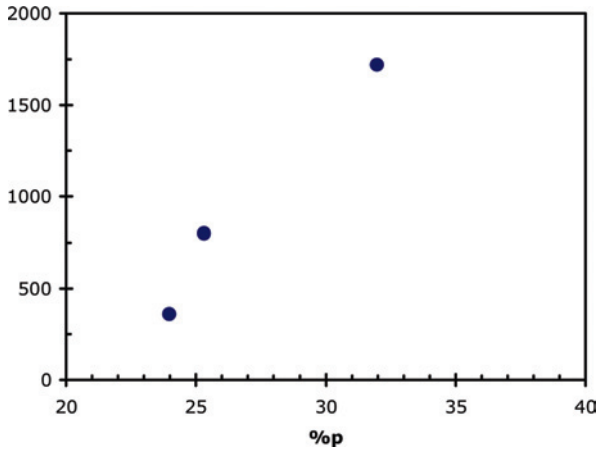

Figure 8. Calculated ^{207}Pb shielding spans for the three $Pb(L)_x[Au(CN)_2]_2$ polymers **1**−**3** and the percent of lone pair in p-orbital.

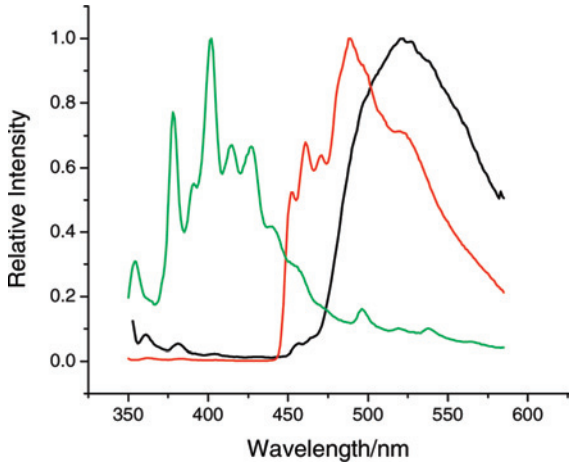

Figure 9. Luminescence spectra at 77 K of $Pb(phen)_2[Au(CN)_2]_2$ (black), $Pb(phen)_2[ClO_4]_2$ (red), and phenanthroline ligand (green).

luminescence of **1** to lead, gold, or ligand-based luminescence, analogous spectra of $[Pb(phen)_2](ClO_4)_2$ were measured (Figure 9-red), and they showed very similar emission maxima (λ_{em} = 490 nm) and excitation maxima (λ_{ex} = 342 nm) to **1**. Thus, we assign the luminescence observed for **1** as due to the $[Pb(phen)_2]^{2+}$ unit and to be due to a lead-to-ligand transition. The absence of any aurophilic interactions in **1** implies that no strictly cyanoaurate-based luminescence should be observed.[89] Note that the emission spectrum at

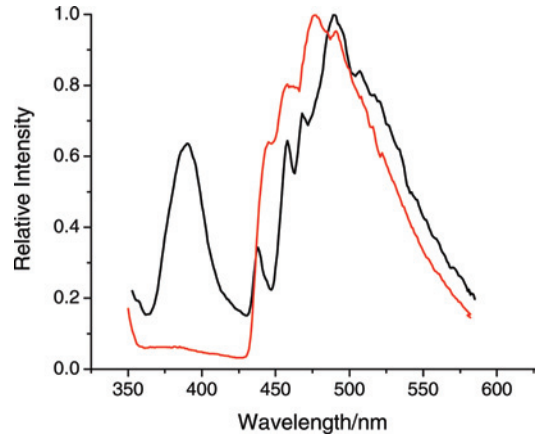

Figure 10. Luminescence spectra at 77 K of $Pb(bipy)_2[Au(CN)_2]_2$ (black) and $Pb(bipy)_2[ClO_4]_2$ (red).

77 K for the phenanthroline ligand itself (λ_{em} = 391, 412, 437, 466 nm with λ_{ex} = 345 nm; Figure 9-green) is quite distinct from either Pb-containing complex in Figure 9.

The luminescence spectrum of **2**, $[Pb(bipy)_2][Au(CN)_2]_2$, at 77 K is shown in Figure 10-black. It consists of a broad emission peak at 494 nm with an excitation maximum at 334 nm. This is very similar to the luminescence spectrum at 77 K for the simple complex $[Pb(bipy)_2](ClO_4)_2$ shown in Figure 10-red with λ_{em}^{max} = 475 nm and λ_{ex}^{max} = 320 nm. Thus, the emission band at 494 nm for **2** is assigned to a Pb-to-bipy transition. An additional emission peak at 390 nm with λ_{ex} = 340 nm is observed and attributed to $[Au(CN)_2]^-$ units with a weak aurophilic interaction. A similar emission at 390 nm (λ_{ex} = 337 nm) is observed for $KAu(CN)_2$,[89] which has an Au−Au nearest neighbor distance of 3.64 Å, comparable to that found in **2**. The bipyridine ligand has a luminescence maximum at 360 nm with λ_{ex}^{max} = 325 nm, which is dissimilar to the spectra in Figure 10.

In the emission spectrum (Figure 11-black) of the ethylenediamine-containing polymer **3**, which does contain significant metallophilic interactions, a shoulder at 408 nm and a peak at 440 nm (λ_{ex} = 340 nm) is observed. Figure 11-red shows the luminescence spectrum of $Pb(NO_3)_2$ with an emission band maximum at 448 nm with 340 nm excitation and is assigned to a Pb^{2+} transition (6p → 6s); the luminescence of $Pb(H_2O)[Au(CN)_2]_2$ was analyzed in a

(89) Nagasundaram, N.; Roper, G.; Biscoe, J.; Chai, J. W.; Patterson, H. H.; Blom, N.; Ludi, A. *Inorg. Chem.* **1986**, *25*, 2947.

(90) Patterson, H. H.; Bourassa, J.; Shankle, G. *Inorg. Chim. Acta* **1994**, *226*, 345.

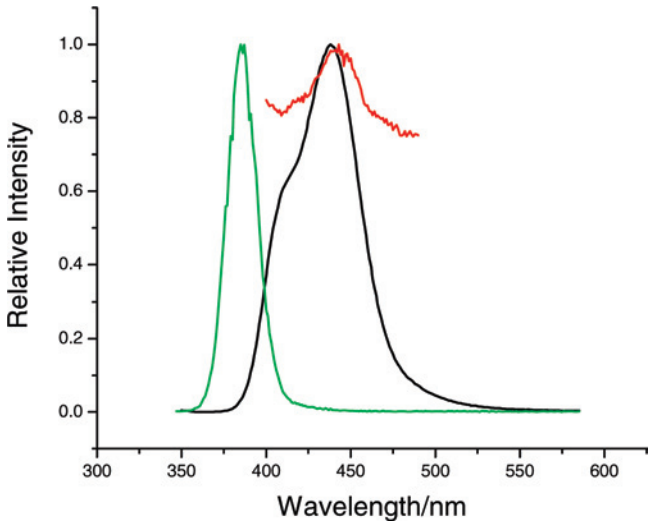

Figure 11. Emission and excitation spectra at 77 K of $Pb(en)_2[Au(CN)_2]_2$ (black), $Pb(NO_3)_2$ (red), and $KAu(CN)_2$ (green).

similar fashion.[90] Because of the similarity of the 440 nm band to the transition observed in $Pb(NO_3)_2$, we believe that there is a strong Pb^{2+} contribution to this transition. Accordingly, it is assigned to a Pb—Au transition (also, see calculations below). Figure 11-green shows the emission peak at 390 nm for $KAu(CN)_2$. Thus, in Figure 11-black the 408 nm shoulder is assigned to a Au—Au transition with the Pb $6p_z$ orbital contributing to the LUMO and resulting in a decrease in the HOMO—LUMO energy in comparison to $KAu(CN)_2$. Because Tl^+ and Pb^{2+} both have lone pairs, the rationale behind the shifted Au-based luminescence of **3** should be comparable to the previously reported $TlAu(CN)_2$ complex. Extended Hückel and ab initio MO calculations for $TlAu(CN)_2$ indicated that the LUMO in this case has a composition of mostly CN^- π^* character and an admixture of Tl 6p orbitals resulting in the lowering of the LUMO,[91,92] and a similar situation appears to be present in **3**.

Single point DFT calculations have been carried out for models of **3** to understand the contribution of Au—Au and Pb—Au interactions to the luminescence spectra. The geometry of compound **3** was taken from crystallographic data and all the bond lengths, bond angles, and dihedral angles were frozen. Several models for **3** were considered, and the results are tabulated in the Supporting Information. One model shown here corresponds to a segment of the polymeric chains of **3** that include the short Pb—Au and Au—Au interactions. The HOMO, LUMO, and LUMO+2 of **3** are

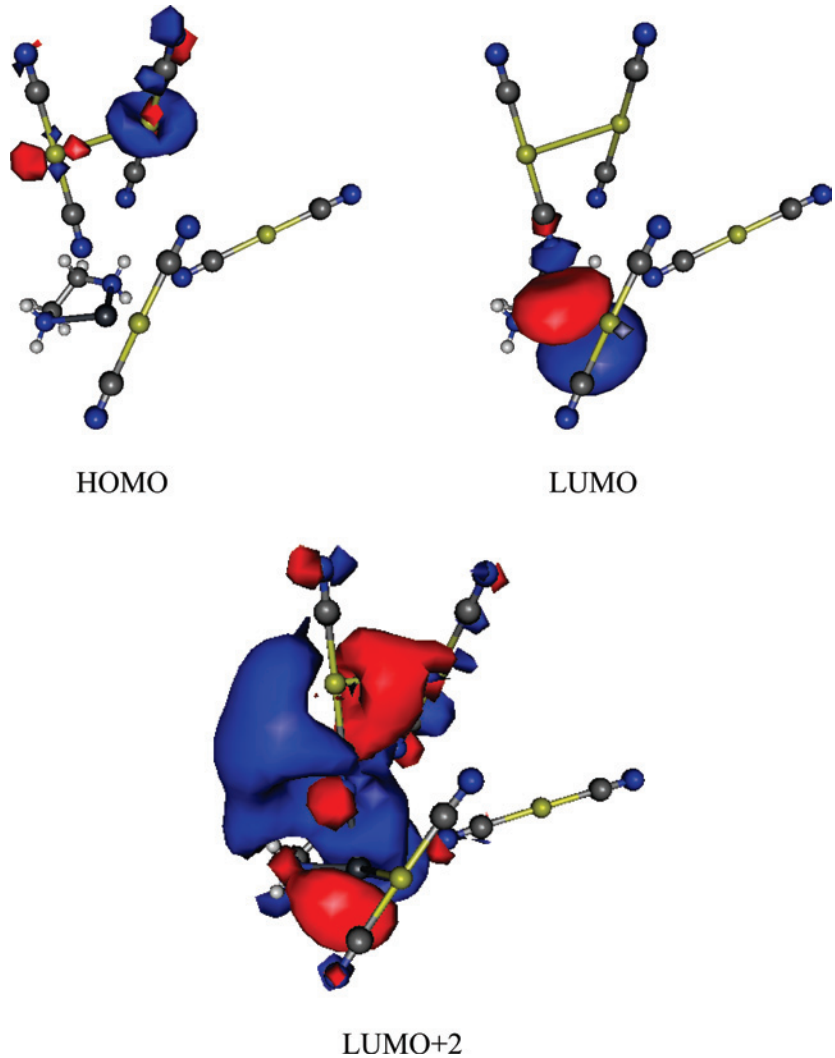

Figure 12. Molecular orbitals of $Pb(en)[Au(CN)_2]_2$ showing the HOMO, LUMO, and LUMO+2 states.

Table 6. Population Analysis for **3**

MO	% Pb(en)	% $Au(CN)_2^-$	energy/eV
105	0.12	99.88	−2.4860
106	1.85	98.15	−2.4585
107	0.07	99.93	−2.3358
108	0.11	99.89	−1.9450
109	0.04	99.96	−1.9148
110 (HOMO)	0.17	99.83	−1.6778
111 (LUMO)	69.46	30.54	1.4242
112	60.07	39.93	2.3080
113	20.96	79.04	3.2762
114	27.27	72.73	3.4133
115	15.54	84.46	3.7374
116	6.42	93.58	3.9028

shown in Figure 12. Note that the composition of the HOMO is $Au(CN)_2^-$ while the LUMO is mostly Pb with some contribution coming from the Au. Population analysis (Table 6) showed that the HOMO is 99.8% $Au(CN)_2^-$ and 0.2% Pb(en) while the LUMO is 30.5% $Au(CN)_2^-$ and 69.5% Pb(en). The LUMO+2 consists mostly of $Au(CN)_2^-$ (79.02%), with a 20.96% contribution from the Pb(en) moiety. The same trend is seen in the different models that were considered, in which the HOMOs are comprised of $Au(CN)_2^-$ while the LUMOs are comprised mostly of the Pb(en) moiety with a contribution from the $Au(CN)_2^-$ that vary from 20 to 30%. This is supportive of the observed 440 nm peak in **3** that is assigned to a Pb−Au transition and the 408 nm peak that is assigned to a Au−Au transition. This is a similar situation to the case of the heterometallic mixed metal system, $K[Au_xAg_{1-x}(CN)_2]$ ($x = 0 \rightarrow 1$), where a Ag−Au transition was observed.[93] In addition, ab initio relativistic MO calculations for $Tl_2Pt(CN)_4$ indicate substantial σ orbital overlap between the 6s and $6p_z$ valence orbitals of Tl and the $5d_{z^2}$ and the $6p_z$ orbitals of Pt. These theoretical results suggest a high degree of Tl(I) lone pair stereochemical activity resulting in luminescence from states which are a mixture of both Tl and Pt rather than from Pt states alone.[92]

In summary, the luminescence measurements for **3** demonstrate the existence of Au−Au and Au−Pb interactions and are consistent with the high degree of Pb(II) lone pair stereochemical activity. For compounds **1** and **2** with limited lone pair stereochemical activity we do not observe in luminescence the presence of a Pb−Au transition.

Conclusion

Three coordination polymers containing lead(II), $[Au(CN)_2]^-$, and chelating N-donor ligands have been synthesized and structurally characterized. An increase in ligand basicity increases the degree of sp-hybridization, or stereochemical activity, of the Pb(II) lone pair, as indicated by a concomitant increase in the variation of the Pb(II)−N bond lengths (determined from X-ray crystallography) and an increase in the span and position of the chemical shifts in the solid-state ^{207}Pb MAS NMR spectra. The combination of ^{207}Pb MAS NMR and relativistic theoretical calculations, as well as the luminescence measurements, each clearly provides valuable spectroscopic insight into the nature of the stereochemical activity of the lone pair in these lead(II) coordination polymers. Nonstructural probes for lone pair activity such as the NMR and luminescence data presented herein are very rare.

The controllable tuning of the lone pair's impact on the coordination sphere of the lead(II) center is a useful tool for influencing the supramolecular structures, and therefore the properties, of lead(II) coordination polymer materials. For example, by generating a formally low-coordinate Pb(II) coordination sphere in **3** by toggling on the lone pair activity with the basic ethylenediamine ligand, the ease of formation of a Pb−Au interaction was likely enhanced. In addition to structural evidence, the presence of this rare metal−metal interaction was substantiated by luminescence measurements and calculations that attributed emissions to the Pb−Au and Au−Au interactions.

Overall, these results can be used to guide the design of other Pb(II)-containing polymers with the goal of improving the physical and optical properties of this important class of materials.

Acknowledgment. Financial support from NSERC of Canada (D.B.L., S.K., M.J.K.) and from the National Science Foundation Grant CHE-0315877 (H.H.P.) is gratefully acknowledged. The Varian Inova 600 and Thermo Nicolet Nexus 670 FT-Raman spectrometers (University of Manitoba) are supported by the Canada Foundation for Innovation and the Province of Manitoba. We are grateful to Dr. Gabriele Schatte (Saskatchewan Structural Sciences Center) for collecting the X-ray crystallographic data for **3**.

Supporting Information Available: Composite X-ray crystallographic file (CIF) for **1**−**3**, population analysis for MOs of various models of **3**, comparisons of simulated and experimental ^{207}Pb MAS NMR spectra for **1**−**3**, and complete reference 65 (PDF). This material is available free of charge via the Internet at http://pubs.acs.org.

IC800425F

(91) Assefa, Z.; DeStefano, F.; Garepapaghi, M. A.; LaCasce, J. H., Jr.; Ouellette, S.; Corson, M. R.; Nagle, J. K.; Patterson, H. H. *Inorg. Chem.* **1991**, *30*, 2868.
(92) Ziegler, T.; Nagle, J. K.; Snijders, J. G.; Baerends, E. J. *J. Am. Chem. Soc.* **1989**, *111*, 5631.
(93) Hettiarachchi, S. R.; Schaefer, B. K.; Yson, R. L.; Staples, R. J.; Herbst-Irmer, R.; Patterson, H. H. *Inorg. Chem.* **2007**, *46*, 6997.